International Journal of Tomography & Statistics,
Summer 2008, Vol. 9, No. S08; Int. J. Tomogr. Stat.; 1-11
ISSN 0972-9976 (Print); ISSN 0973-7294 (Online)

A novel up-to-down algorithm for road extraction

David Tien[1], **Yi Xiao**[1] **and Qing-hua Qin**[2]

[1]School of Information Technology
the University of Charles Sturt
Bathurst, NSW 2795, Australia

[2]Department of Engineering
the Australian National University
Canberra, ACT 0200, Australia

ABSTRACT

On the basis of the symmetric axis transform (SAT), the constrained Delaunay triangulation (CDT) technique, and a split-and-merge approach, a new 'up-to-down' algorithm is developed to identify various roads from aerial images. The contours (shapes) of all the potential road regions that are segmented from aerial images are represented by their SAT for decomposing these regions into parts, so that the linear features of the shapes such as the length, width and curvature can be quantitatively measured on the parts, while CDT technique is applied to implement the SAT in discrete domain. From the CDT, the length and width for each part can be computed, and a split-and-merge algorithm is applied for calculating the curvature of each part. Three rules are proposed in terms of the width, length and curvature to identify roads from the candidature road regions. The study shows that the proposed technique is a promising algorithm for identifying roads from aerial images and appears to be superior to the existing methods in that it can extract road networks under complex background with less artifacts. Moreover, as the symmetry based method can quantitatively describe roads, it is also a useful tool for road vectorization.

Keywords: road extraction, symmetry axis transform, curvature calculation.

2000 Mathematics Subject Classification: 68U10, 62M40, 62H35.

1 Introduction

The automated extraction of road networks from aerial images is one of the challenges in remote sensing and computer vision community. Various approaches for road extraction have been proposed during the past decades and most existing approaches for road extraction are in the so-called 'bottom-to-top' way from grayscale or infrared images (Zhang, 2004). With these methods, salient points in roads or small portions of roads are located and the whole roads are traced from these points/portions based on some geometrical constraints. Fischler et al. (Fischler, Tenenbaum and Wolf, 1981) first extracted reliable hypotheses for road segments through line and edge detection and then established connections between road segments to form road networks. McKeown and Denlinger (McKeown and Denlinger, 1988) and Vosselman and Knecht (Vosselman and de Knecht, 1995) presented approaches starting from a given point and a given direction after extracting parallel edges or by extrapolating and matching profiles in high-resolution images. Merlet and Zerubia (Merlet and Zerubia, 1996) connected points using dynamic programming. They characterized roads with the derivatives of the gray values, straight lines or smooth curves, normally circular arcs, and their local curvature and used an optimization program for road recognition. Neuenschwander et al. (Neuenschwander, Fua, Székely and

Kübler, 1995) used so-called “ziplock snakes” which provide means to connect given points in the presence of obstacles.

For more complicated road structures, Barzohar and Cooper (Barzohar and Cooper, 1996) created a geometric-stochastic model for road description and detected roads by maximum posteriori probability estimation. Gruen and Li (Gruen and Li, 1997) developed a LSB-Snake method to connect points for reconstructing roads simultaneously in multiple images. Baumgartner et al. (Baumgartner, Steger, Mayer and Eckstein, 1997) used the scale-space behavior of roads to grouping roads into network. Zhang and Baltsavias (Zhang and Baltsavias, 2000) utilized multiple cues about the object existence and employed existing knowledge, rules and models for road network reconstruction from aerial images, in order to increase success rate and reliability of the results.

Despite many efforts have been made toward road analysis during the past decades, developing reliable algorithms for road network extraction remains a challenging task, and there is lack of algorithms that are sufficiently robust and accurate for practical use (Xiong, 2001). Recently, road detection in an ’up-to-down’ way has drawn attention by many professionals. Clode et al. (Clode, Rottensteiner and Kootsookos, 2005) proposed an ‘up-to-down’ method for road detection. They extracted all the possible road regions from LIght Detection And Ranging (LIDAR) data and multi-spectral image fusion, then removed the non-road regions by checking the sizes of individual regions (connected components). Mokhtarzade and Valadan Zoej (Mokhtarzade and Valadan Zoej, 2007) presented another up-to-down method that applied artificial neural networks for road detection from high-resolution satellite images. A variety of network structures with different iterations are used to determine the best network structure and termination condition in training stage. Verification was made for the impacts of different input parameters on network’s ability to find out optimum input vector for the problem. The two ‘up-to-down’ methods are insensitive to the variations of road conditions and the structures of road network. However, the major drawbacks are the presence of many artifacts caused by the objects such as car parks and private roads that link to the main roads. With these pixel-based methods, the artifacts are difficult to be removed from the main road regions. To solve this problem, Zhang and Couloigner (Zhang and Couloigner, 2006) proposed a road identification approach integrating k-means clustering and a fuzzy logic classifier. A number of shape descriptors of angular texture signature are introduced for separating roads from car parks. The limitation is the retaining of the small artifacts. We apply the symmetric axis transform (SAT) (Blum, 1967; Blum and Nagel, 1978) for road region presentation. The novelty of the proposed method is the utility of the vectorized analysis instead of the existing pixel based analysis. This makes it available to handle the artifacts based on partial regions. Symmetric axis transform is an intriguing tool for analyzing and computing of elongated shapes in vectorization format. It extracts thinned features of a shape, and therefore, has been widely used for elongated shape representation and analysis such as Chinese character extraction (Zou and Yan, 2001), optical character analysis (Xiao and Yan, 2004), document image analysis (Xiao and Qin, 2005) and the geographic information system (Gold, Thibault and Liu, 1999). In this paper, SAT is conducted on the contours (shapes) of the candidature road regions that are segmented from aerial images. The SAT decomposes a region into parts (components) and keeps the topological information of the region. The roads are extracted by measuring the linear features of these components, such as the width, length and curvature. From these linear feature calculations, three rules are then generated for artifact identifying, therefore, the artifacts can be pruned.

The rest of the paper is organized as follows: Section 2 provides a brief description of SAT and CDT and its discrete implementation by CDT and their applications to analyse linear features of an elongated shape. The component curvature computing using the split-and-merge method is discussed in Section 3. Section 4 describes some rules with which artifacts are pruned. Finally, numerical results are presented to assess the proposed algorithm in Section 5.

2 Shape's length and width measurement

2.1 Symmetric axis transform and its discrete presentation

The SAT of a shape is defined as the locus of the centers and the radii of all *maximal disks* contained in the shape. A maximal disk contained in the shape is any circle with its interior contained in the shape such that the circle touches the boundary of the shape at two or more points (see Figure 1). The locus of the centers constitutes the *symmetric axis*(SA). The centers consist of three types of SA points: *end points*, *normal points* and *junction points*. A SA point having one contact point from its *maximal disk* to the boundary of the shape is an *end point*. *Normal points* are SA points having two contact points from its *maximal disk* to the boundary of the shape, and *junction points* are points with three or more contact points from its *maximal disk* to the boundary of the shape (see Figure 1).

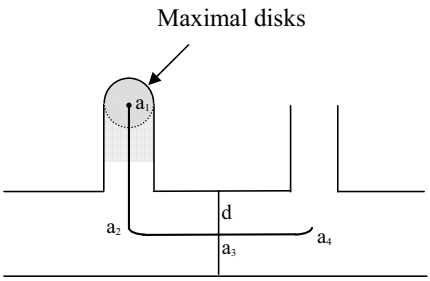

Figure 1: Illustration of symmetric axis points, maximal disks, a branch and a trunk. a_1 is an end point, a_3 is a normal point, a_4 is a junction point.

The symmetric axis is, then, divided into simplified segments in terms of different types of SA points. This permits a complex shape to be split into several simpler parts that may be quantitatively described. A typical part (*simplified segment* in Blum's description) is defined by a set of continuous normal points bounded by either a junction point or an end point. In the symmetric axis, we call a subset of the continuous centers ending with an end point and a junction point a *branch*, and a subset of the continuous centers ending with two junction points a *trunk*. In Figure 1, for example, a_1 is an end point, a_2 and a_4 are junction points, and a_3 is a normal point. a_1a_2 is a branch, a_2a_4 is a trunk.

In the discrete domain, on the other hand, SAT can be described using the CDT technique (Chew, 1987). Given the contours of a shape, the CDT of the shape is a constrained triangulation where the circumcircle of each triangle does not contain in its interior any other vertex which is visible from all the vertices of the triangle. A triangle of the CDT of a shape here refers to a triangle lies entirely inside the shape. An edge of a triangle is an *external edge* if it is on the contour. Otherwise, it is an *internal edge*. A triangle with one, two, or three internal edges is called, respectively, an *end-triangle* (***ET***), a *normal-triangle* (***NT***), or a *junction-triangle* (***JT***). The centroid of an ***ET*** and a ***JT*** is an end point and a junction point respectively. The mid-point of an internal edge in a ***NT*** is a normal point (Zou and Yan, 2001).

A shape in the discrete SAT is decomposed into components by ***ET***s and ***JT***s. A component consists of a chain complex of internal-edge-shared triangles, of the form ***ET NT .. NT JT***/ ***JT NT .. NT ET***, ***JT NT .. NT JT*** or ***ET NT .. NT ET*** relating to a branch and a trunk in SAT.

With this discrete description, roads are divided into segments cut by intersections or T-junctions. That is, a component represents a road section between two intersections/T-junctions or an intersection/T-junction and an end of roads or a road without intersections and T-junctions.

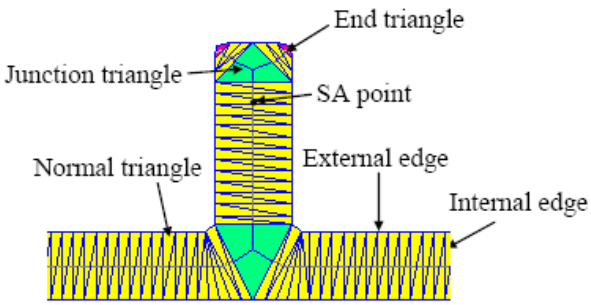

Figure 2: End triangle (***ET***), normal triangle (***NT***) and junction triangle (***JT***) and internal edge, external edge and SA point.

2.2 Shape's length and width calculation via Delaunay triangulation

A *local object width* is the length of an internal edge in a ***NT*** in the discrete domain ((Zou and Yan, 2001), see Figure 2 for illustration). While *component width* (w_c) is defined as the dominant local object width in a component.

Let w_a be the length at the maximum peak in the histogram of local object width, we have

$$w_c = w_a \tag{2.1}$$

For an elongated shape with uniform widths, its local object widths are distributed around w_c.

Component Length (L_c) is defined as the total lengths of the line segments in a component. The two end points of a line segment e_i are the two normal points in a ***NT***. Then, we have

$$L_c = \sum_N e_i. \tag{2.2}$$

Table 1 lists the component width and length for different shapes found in candidature road regions.

Table 1 Component width and length for different shapes

Component	w_c, w_m	L_c	Component	w_c, w_m	L_c
(1)	114, 148	1381	(7)	115, 182	1344
(2)	147, 217	1351	(8)	114, 267	1735
(3)	98, 132	1383	(9)	147, 187	700
(4)	179, 179	880	(10)	164, 316	658
(5)	98, 125	995	(11)	393, 477	1068
(6)	98, 181	2188	(12)	164, 316	986

w_m is the maximum local object width.

An elongated shape shown in Table 1, is featured with narrower component width and longer component length. Components $1 \sim 7$ in the table are cut from road sections. They have relatively longer component lengths and narrower maximum local object widths. Most of them have a length greater than 990 and maximum local object width less than 220. Components $8 \sim 12$ are from the private roads, car parks and small paths. Their maximum local object widths are greater than 260, excluding component 9 that has a comparable width to road section's width.

3 Component curvature analysis

To tackle various artifacts that have comparable widths and lengths with roads, a split-and-merge algorithm is used to calculate component curvatures and therefore identify the corresponding results.
The split-and-merge algorithm presented in (Duda and Hart, 1973; Pavlidis and Horowitz, 1974; Wu and Leou, 1993; Pikaz and Dinstein, 1995) is a commonly used method for high curvature point extraction in a curve. The algorithm extracts a sub-set of the curvature points along the curve. The main function of a split-and-merge algorithm is to test for collinearity. The split procedure is a recursive process. At each stage, the point which has the maximum distance from the chord determined by the two end-points, is chosen. Denote the endpoint by a, b and the selected point by c. The point a, b and c are chosen to be part of the approximation vertices. The next recursive step is with the two sub-curves confined by a, c and by b, c. The process is proceeded as long as the distance between the selected point and the corresponding chord is greater than a given tolerance ε. The merge procedure is based on linear scan. The curve is scanned while each point is merged with the current segment if their union is sufficiently close to a straight line, otherwise that point is the beginning of the next segment. The split-and-merge algorithm conducts the split and merge iterations until no reductions of the vertices number occurs.
A curve will be distorted if the value of ε is too large. Conversely, if the value of ε is a too small some noise will remain in the curve. In the experiment, best results for a curve are obtained when ε is between $10 \sim 20$. For a given ε, a curve with lower radian will have less curvature points and longer straight line segments.
In addition, we define a 'straightness ratio' to statistically measure the straight line segments of a curve in its high curvature point extraction. Let $P = \{p_j(x_j, y_j)\} \quad j = 1, 2, \ldots, m$ be an ordered sequence of high curvature points in a curve after the splitting and merging algorithm, and $PE = \{E_k\}$, $k = 1, 2, \ldots, m$, where $E_k = |p_k - p_{k+1}|$ is the length of two consecutive points in P.
The 'straightness ratio' is, then, defined as

$$r = \frac{S_S}{S_L}, \tag{3.1}$$

where $S_L = \sum_{k=1}^{m} E_k$ and $S_S = \sum_{k=1}^{m} E_k | E_k > th_E$. th_E is the length threshold, and r reflects the radians of a curve.
Table 2 shows the measurement of r for different curves obtained in candidature road regions. Components $1 \sim 7$ are manually classified as road sections and components $8 \sim 12$ as artifacts such as driveways and car parks. From Table 2 we can see that r is directly proportional to ε and inversely proportional to th_E. Longer curves with lower radian have larger values of r. When $th_E = 15$, we can set a cut off value (th_r) of r ($th_r = 0.65$ at $\varepsilon = 10$ or $th_r = 0.8$ at $\varepsilon = 20$) for separating components $1 \sim 7$ from components $8 \sim 12$. When $th_E = 22$, value of r for component 3 is smaller than the values of r for components 7, 8, 9 and 11. Components $1 \sim 7$ can't be classified into one group in terms of the values of r.
To investigate the effect of th_E on the separation of road regions from artifacts, we evaluate different r in terms of th_E and ϵ, as illustrated in Figure 3(a) and Figure 3(b).

Table 2 *r* for different curves (th_E =15, 22 , ε=10, 20)

Component	th_E=22 ε=20	th_E=15 ε=20	th_E=22 ε=10	th_E=15 ε=10	Component	th_E=22 ε=20	th_E=15 ε=20	th_E=22 ε=10	th_E=15 ε=10
(1) 	0.66	0.94	0.64	0.82	(7) 	0.88	0.96	0.79	0.87
(2) 	0.73	0.89	0.35	0.73	(8) 	0.47	0.67	0.37	0.63
(3) 	0.73	0.90	0.73	0.90	(9) 	0.62	0.80	0.30	0.45
(4)	0.83	0.83	0.83	0.83	(10) 	0.22	0.57	0.22	0.39
(5) 	0.46	0.90	0.39	0.68	(11) 	0.51	0.77	0.37	0.63
(6) 	0.83	0.96	0.83	0.96	(12) 	0.14	0.58	0	0.45

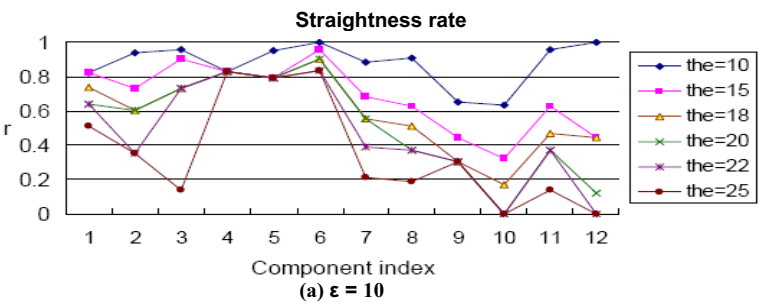

(a) ε = 10

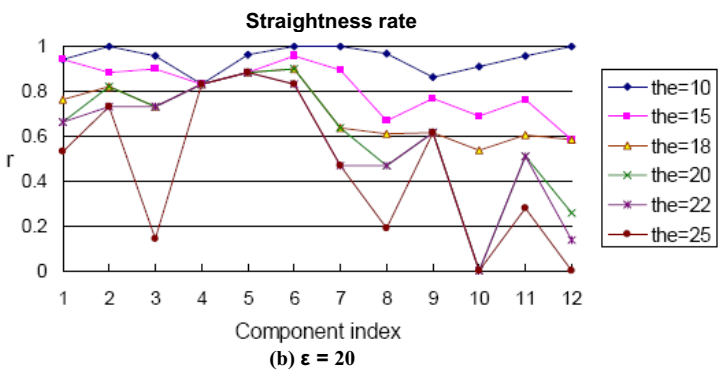

(b) ε = 20

It can be seen from Figure 3 that, for both $\varepsilon = 10$ and $\varepsilon = 20$, when $15 \leq th_E \leq 20$, the value of r for any component in road regions is greater than the value of r for any component of artifacts in Table 2; when $th_E < 15$, the values of r for some components of artifacts are greater than the values of r for some components of road regions in Table 2 because S_L counts some short line segments in a high radian curve in the calculation based on equation (3.1); when $th_E > 20$, the values of r for some components of road sections (component 3 for example) decreases greatly because of their higher radians than other road sections in Table 2.

4 Road extraction by SAT calculation

During the process of road extraction, the road regions are extracted from the candidature road regions that are the segmentation results of an aerial image. The SAT is carried out on the contours of the candidature road regions. The road candidates are decomposed into components. For each component, its length, width, maximum local object width and curvature are computed as discribied in Sections 2 and 3. Following three rules are proposed here to judge if a component is a road section:

Theorem 4.1 (Rule 1). *Let B be a component of the form **ET NT .. NT JT** or **JT NT .. NT ET**, if $L_c(B) < th_{L1}$ or $w_c(B) < th_{w1}$, B is not a road section. Where $L_c(B)$ is the component length of B, $w_c(B)$ is the component width of B. th_{w1} is the minimum width of roads. th_{L1} is the minimum length of roads.*

This rule is set to remove narrow and short objects such as small paths.

Theorem 4.2 (Rule 2). *Let B be a component of the form **ET NT .. NT JT** or **JT NT .. NT JT**, if $w_m(B) > th_{w2}$, $L_c(B) < th_{L2}$, B is not a road section. Where $w_m(B)$ is the maximum local object width of B. th_{w2} and th_{L2} depend on the maximum width of roads and the maximum length of carparks respectively.*

This rule set is to delete broad and short objects such as car parks or some open space.

Theorem 4.3 (Rule 3). *Let B be a component of the form **ET NT .. NT JT** or **ET NT .. NT ET**, P be the set of SA points for B after split-and-merge calculation. If $r(P) > th_r$, B is regarded as a road segment. Where $r(P)$ is the straightness ratio of P.*

With this rule, some artifacts having the comparable sizes but different curvatures with roads can be deleted.

5 Experiment and discussion

The LIDAR data from Fairfield in Sydney, Australia, with an average point density of one point per 1.3m^2 was used in road region segmentation, together with a true colour digital orthophoto with a resolution of 15cm for the same area. The Fairfield data is a typical data set for testing. It has both residential and industrial urban regions present within a $2000 \times 2000\text{m}^2$ area. There are buildings, roads, car parks, trees and vegetation as well as a treed creek area.

5.1 The procedure of road detection

The road extraction follows road region segmentation. A road segmentation algorithm is, here, developed based on the Clode et al's method. The difference between the Clode et al's method and the proposed algorithm is that, in the proposed algorithm, the spectral image is replaced by the colourful orthophoto that is more accessible. The road samples library in colour space is established for road

segmentation. Road regions are segmented from background by comparing the distance of each pixel in colour space to the element in road sample library (see (Xiao and Tien, 2006) for details). The final road candidatures are the overlay of the road segmentation from LIDAR data and colourful orthophotos. All the main roads and many private roads are separated from the background, together with regions containing materials similar to roads in colors. Some fragments occur as the result of shadows and vehicles presenting on the roads.
The procedure of road extraction with the Fairfield data set are illustrated in Figure 4.

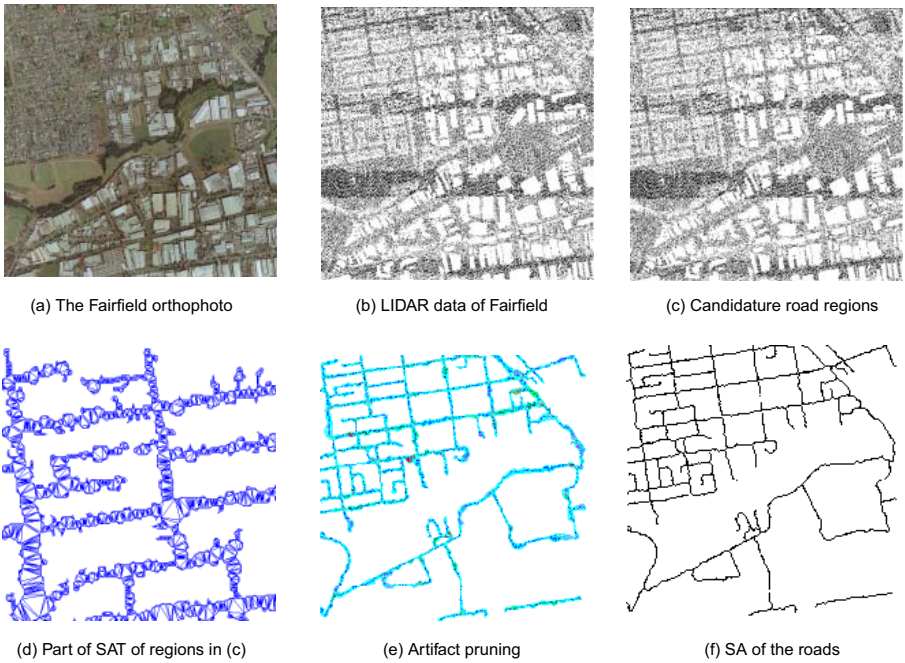

(a) The Fairfield orthophoto (b) LIDAR data of Fairfield (c) Candidature road regions

(d) Part of SAT of regions in (c) (e) Artifact pruning (f) SA of the roads

Figure 4: The procedure of road extraction.

5.2 The results and discussion

The discussion focuses on the following three aspects:
(i) *The effect of the parameter values.* A number of thresholds are used in the pruning rules as shown in Table 3. The values of th_{w1}, th_{w2}, th_{L1} and th_{L2} depend on the ranges of road lengths and widths. th_{L1} is set for pruning small paths and private roads. The value change of th_{L1} is sensitive to the results. If th_{L1} is too large, it will cause missing of some end road segments, while if th_{L1} too small, it will retain some small paths. In the experiment, we found that $th_{L1} = 80$ is optimum for achieving satisfying extraction accuracy.
th_r, ε and th_E are for road straightness measuring. The choice of ε aims at suppressing the noise along the curve while retaining the shape information of the curve. th_E depends on the tolerance of road curvature. The value increasing of th_E may lead to eliminating of roads with high radians; a decrease in the value of th_E may cause the preservation of some artifacts. The detailed discussion on this issue was already given in Section 3.
(ii) *The effect of the road segmentation.* As the segmentation of the road regions is partially based on

Table 3: Threshold values for pruning.

th_{w1}	th_{L1}	th_{w2}	th_{L2}	th_r, ε, th_E
80	400	320	1400	0.65, 10, 15

the colour of the surveyed area, tree shadows can cause road fragmentation. The short fragments will be deleted by the succeeding processing. An example is shown in the horizontal road in the southern part of Figure 4(a). It is broken in the binarized image shown in Figure 4(b).

As private road sections have the same colours with some main road sections, some private roads being the extension of main roads can not be separated from the main roads by the pruning processing.

(iii) *Comparison.* To evaluate the obtained results, *completeness* and *correctness* similar to those in (Clode et al., 2005) are used, but we compute the metrics on a length basis instead of a pixel basis. *completeness* and *correctness* are defined as follows:

$$completeness = \frac{TP}{TP + TN} \qquad correctness = \frac{TP}{TP + FP}$$

TP (True Positive) is the road length detected manually and by the algorithm, FP (False Positive) is the road length detected by the algorithm but not manually, and TN (True Negative) is the road length detected manually but not by the algorithm. *completeness* measures the recall of a method to find the road regions. *correctness* measures the precision of a method for road detection.

For the consistency of comparison, we adopt Clode's segmentation as candidature road regions for road extraction (See Figure 5). Table 4 shows the *completeness* and *correctness* of Clode's and our methods. We can see from Table 4 that both Clode's method and ours have high *completeness*. That means both methods can extract the roads with complex structures. The missed road segments in our results are the short road segments caused by small road fragments or the cutting of the roads in the boundary of the image. The *correctness* of our method is much higher than the one of Clode's method. As the short and fat artifacts or the artifacts with high radians linked to the roads are pruned in our method, only the private roads that have the same widths and segment lengths with main roads are retained (See Figure 5).

Table 4: *completeness* and *correctness*.

	completeness	*correctness*
Clode's method	0.97	0.87
Our method	0.95	0.97

Also, comparing to Clode et al's method, the database we used is more accessible. Furthermore, road information such as centerlines, sections and intersections can be obtained from the resultant extraction by the SAT.

6 Conclusion

This paper proposes a symmetry based method for road extraction from aerial images. By representing the potential road regions with their SAT of the region's contours, calculating the length and width of each component in the SAT and measuring its curvature via the split and merge algorithm, the roads are identified following three rules that are based on the calculation of the length, width and curvature of the candidature road regions. With our method, artifacts with nonlinear features are removed.

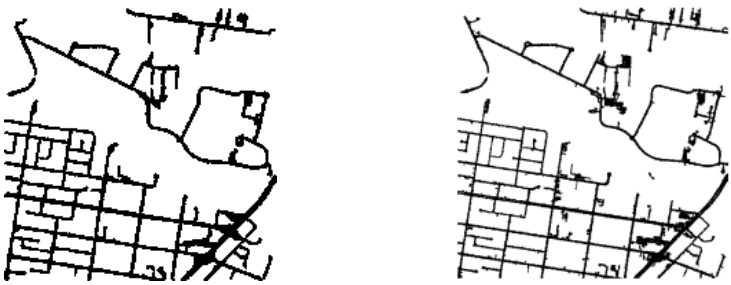

(a) Our method (b) Clode et al's method

Figure 5: Road extraction results.

The main advantages of SAT for road extraction are that (i) road sections and intersections can be obtained form the SAT; (ii) the width, length and curvature of roads can be quantitatively measured; (iii) most of the artifacts around the roads can be removed without morphological changing of the roads; (iv) the extracted roads are vectorized with centerlines by SA points.
As the road extraction relies on the initial segmentation of the road regions, the development of the efficient road segmentation algorithm is expected. And applying the property of proximity of Delanauy triangulation to link broken roads is also a direction for future work.

References

Barzohar, M. and Cooper, D. B. 1996. Automatic finding of main roads in aerial images by using geometric stochastic models and estimation, *IEEE Transactions on Pattern Analysis and Machine Intelligence* **18**(7): 707–721.

Baumgartner, A., Steger, C., Mayer, H. and Eckstein, W. 1997. Multi-resolution, semantic objects, and context for road extraction, *Semantic Modeling for the Acquisition of Topographic Information from Images and Maps* pp. 140–156.

Blum, H. 1967. A transformation for extracting new descriptors of shape, *W. Wathen Dunn (ed) Symposium on Models for the perception of speech and visual form, Cambridge: M. I. T. Press* pp. 362–380.

Blum, H. and Nagel, R. N. 1978. Shape description using weighted symmetric axis features, *Pattern Recognition* **10**: 167–180.

Chew, P. 1987. Constrained delaunay triangulation, *Proc. of the* 3^{rd} *ACM Symp. on Comp. Geometry* pp. 213–222.

Clode, S., Rottensteiner, F. and Kootsookos, P. 2005. Improving city model determination by using road detection from lidar data, *Stilla U, Rottensteiner F, Hinz S (Eds) CMRT05. IAPRS* **XXXVI**(Part 3/W24): 29–30.

Duda, R. O. and Hart, P. E. 1973. *Pattern Classification and Scene Analysis*, Wiley, New York.

Fischler, M. A., Tenenbaum, J. M. and Wolf, H. C. 1981. Detection of roads and linear structures in low-resolution aerial imagery using a multisource knowledge integration technique, *Comput Graphics Image Process* **15**(3): 201–223.

Gold, C., Thibault, D. and Liu, Z. 1999. Map generalization by skeleton retraction, *International Cartographic Association Workshop on Cartographic Generalization* .

Gruen, A. and Li, H. 1997. Linear feature extraction with 3-d lsb-snakes, *Automatic Extraction of Man-Made Objects from Aerial and Space Images (II)* pp. 287–298.

McKeown, D. M. and Denlinger, J. L. 1988. Cooperative methods for road tracking in aerial imagery, *Computer Vision and Pattern Recognition* pp. 662–672.

Merlet, N. and Zerubia, J. 1996. New prospects in line detection by dynamic programmming, *IEEE Trans Pattern Anal Mach Intell* **18**(4): 426–431.

Mokhtarzade, M. and Valadan Zoej, M. J. 2007. Road detection from high-resolution satellite images using artificial neural networks, *International Journal of Applied Earth Observation and Geoinformation* **9**: 32–40.

Neuenschwander, W., Fua, P., Székely, G. and Kübler, O. 1995. From ziplock snakes to velcro*TM* surfaces, *Automatic Extraction of Man-Made Objects from Aerial and Space Images* pp. 105–114.

Pavlidis, T. and Horowitz, S. L. 1974. Segmentation of plane curves, *IEEE Trans. Comput.* **1**(23): 860–870.

Pikaz, A. and Dinstein, I. 1995. Optimal polygonal approximation of digital curves, *Pattern recognition* **28**: 373–379.

Vosselman, G. and de Knecht, J. 1995. Road tracing by profile matching and kalman filtering, *Automatic Extraction of Man-Made Objects from Aerial and Space Images* pp. 265–274.

Wu, J. M. and Leou, J. J. 1993. New polygonal approximation schemes for object representation, *Pattern Recognition* **26**: 471–484.

Xiao, Y. and Qin, Q. H. 2005. Table detection in scanned document images, *International Journal of Tomography & Statistics (IJTS)* **3**: 1–18.

Xiao, Y. and Tien, D. 2006. an made object detection in colour aerial images, *WALIS Forum* .

Xiao, Y. and Yan, H. 2004. Location of title and author regions in document images based on the delaunay triangulation, *Image and Vision Computing* **22**(4): 319–329.

Xiong, D. 2001. Optimization-based method for automated road network extraction, *National Consortium on Remote Sensing in Transportation* .

Zhang, C. 2004. Towards an operational system for automated updating of road databases by integration of imagery and geodata, *ISPRS Journal of Photogrammetry & Remote Sensing* **58**: 166–186.

Zhang, C. and Baltsavias, E. 2000. Edge matching and 3d road reconstruction using knowledge-based methods, *International Archives of Photogrammetry and Remote Sensing* **33**(Part B3/2): 1008–1115.

Zhang, Q. and Couloigner, I. 2006. Benefit of the angular texture signature for the separation of parking lots and roads on high resolution multi-spectral imagery, *Pattern Recognition Letters* **27**: 937–946.

Zou, J. J. and Yan, H. 2001. Skeletonization of ribbon-like shapes based on regularity and singularity analyses, *IEEE TRANSACTIONS ON SYSTEMS, MAN, AND CYBERNETICS—PART B: CYBERNETICS* **31**: 401–410.